https://doi.org/10.5194/egusphere-2025-164
Preprint. Discussion started: 7 March 2025

# The Critical Role of Volatile Organic Compounds Emission in Nitrate Formation in Lhasa, Tibetan Plateau: Insights from Oxygen Isotope Anomaly Measurements

Xueqin Zheng[a], Junwen Liu[a*], Nima Chuduo[b], Bian Ba[b], Pengfei Yu[a], Phu Drolgar[b], Fang Cao[c], Yanlin Zhang[c]

[a] College of Environment and Climate, Jinan University, Guangzhou, 511443, China
[b] Lhasa Meteorological Administration, Lhasa, 850010, China
[c] School of Ecology and Applied Meteorology, Nanjing University of Information Science and Technology, Nanjing 210044, China

[*] Corresponding author: liu.junwen@jnu.edu.cn

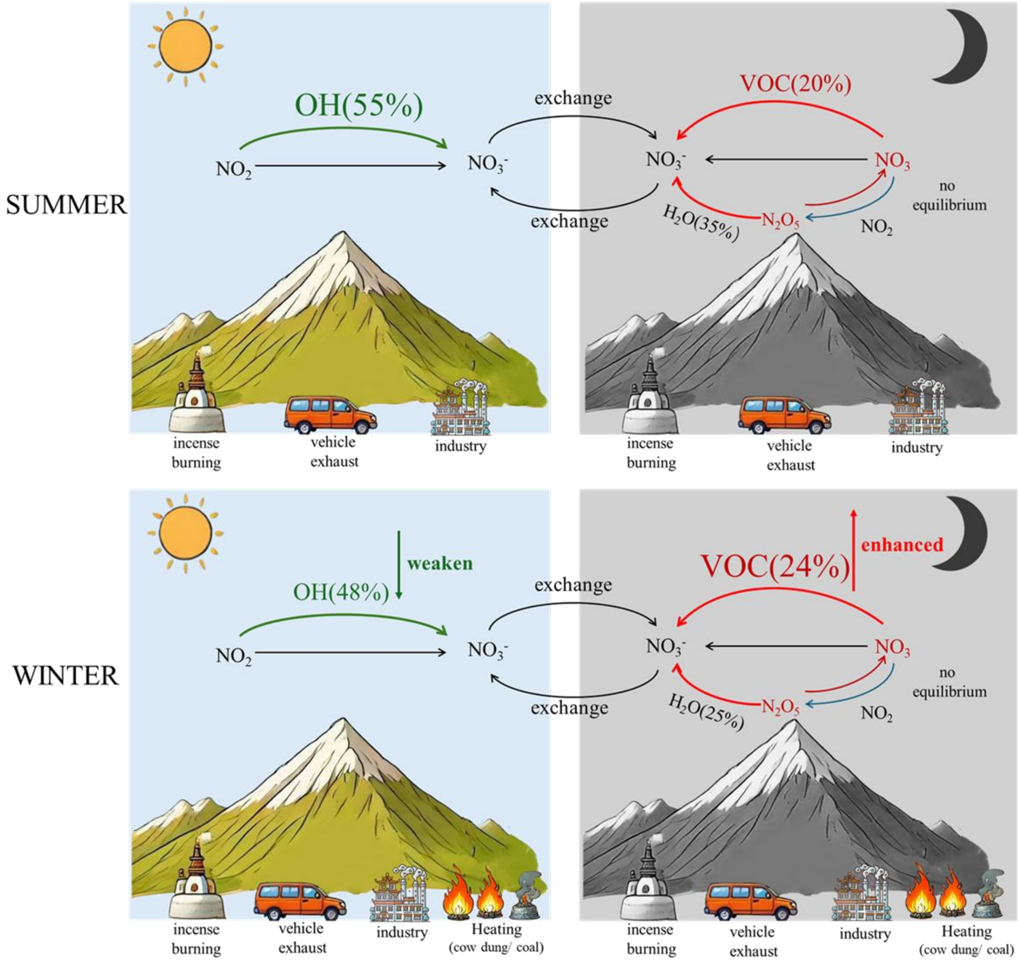
SUMMER
OH(55%)
NO$_2$
NO$_3^-$
exchange
exchange
VOC(20%)
NO$_3^-$
NO$_3$
H$_2$O(35%)
N$_2$O$_5$
NO$_2$
no equilibrium
incense burning
vehicle exhaust
industry
incense burning
vehicle exhaust
industry
WINTER
weaken
OH(48%)
NO$_2$
NO$_3^-$
exchange
exchange
enhanced
VOC(24%)
NO$_3^-$
NO$_3$
H$_2$O(25%)
N$_2$O$_5$
NO$_2$
no equilibrium
incense burning
vehicle exhaust
industry
Heating (cow dung/ coal)
incense burning
vehicle exhaust
industry
Heating (cow dung/ coal)

**TOC art**

## Abstract

Atmospheric particulate nitrate aerosol ($NO_3^-$), produced via the oxidation of nitrogen oxides ($NO_x$ = NO + $NO_2$), plays an important role in atmospheric chemistry and air quality, yet its formation mechanism still poorly constrained the plateau region. In this study, we first reported the yearly variation of the signatures for the stable oxygen isotope anomaly ($\Delta^{17}O = \delta^{17}O - 0.52 \times \delta^{18}O$) in $NO_3^-$ collected in the urban region of Lhasa city (3650 m a.s.l), Tibetan Plateau, China. Our results show that $NO_2$ + OH is the largest contributor to $NO_3^-$ formation (46%), followed by $NO_3$ + VOC (26%), and $N_2O_5$ + $H_2O$ (28%) using the Bayesian Isotope Mixture Model. Notably, there are significant differences in the $NO_2$ + OH, $NO_3$ + VOC, and $N_2O_5$ + $H_2O$ pathways between spring and other three seasons ($p < 0.05$). Our results highlight the influence of VOC emissions from regions such as Afghanistan and northern India, which enhance $NO_3^-$ concentrations in Lhasa during spring. Furthermore, the diurnal distribution of $NO_3^-$ oxidation pathways varied distinctly across seasons, suggesting that these difference in $NO_3^-$ pathways are attributed to ALWC, VOC concentration, and pollution levels.

**Keywords:** nitrate, $\Delta^{17}O$-$NO_3^-$, oxidation pathways, Lhasa, VOC

https://doi.org/10.5194/egusphere-2025-164
Preprint. Discussion started: 7 March 2025

## 1. Introduction

Nitrate aerosol ($NO_3^-$) is a key component regulating the mass concentration of atmospheric fine particulate matter ($PM_{2.5}$), which is highly related with air quality (Colmer et al., 2020), public health (Zhang et al., 2019; Zhang et al., 2017; Geng et al., 2021), and climate system (Clark and Tilman, 2008). Globally, the mass contribution of $NO_3^-$ in $PM_{2.5}$ is in the range of 5-30% (Huang et al., 2014; Xu et al., 2019; Salameh et al., 2015; Espina-Martin et al., 2024; Bell et al., 2007; Sun et al., 2022), depending on the locations and the severities of air pollution. For example, it was reported that $NO_3^-$ accounts for 22%, 27% and 26% in the $PM_{2.5}$ of megacities in China (Zong et al., 2020), Europe (Espina-Martin et al., 2024) and U.S. (Sun et al., 2022), respectively. In addition, some studies found that the contribution of $NO_3^-$ would increase by 3-8 times with the occurrence of the particular-derived haze pollution (Ge et al., 2024; Song et al., 2019; Yin et al., 2022; Walters et al., 2024).

It is well-known that atmospheric $NO_3^-$ is formed by the oxidation of nitrogen oxides ($NO_x$=NO+$NO_2$) with different oxidants such as $O_3$, OH and $RO_2$ (Text S1). In general, atmospheric chemical transportation models are employed to depict the detailed oxidation pathways of $NO_3^-$ formation. However, there are a large uncertainty in modeling the contribution of oxidation pathways to $NO_3^-$ formation using this methodology due to the variable parameters in the real atmosphere. For example, it was reported that the predicted $N_2O_5$ uptake to $NO_3^-$ formation in Beijing, as estimated using WRF-Chem, ranges from 5% to 21% (Su et al., 2017). Higher contributions between 66% and 85% have been observed when applying the CMAQ model in Beijing (Qiu et al., 2019). Therefore, the application of alternative techniques is crucial for providing more reliable estimates and enhancing our understanding of $NO_3^-$ formation mechanisms, in addition to the insights gained from atmospheric chemical transportation models.

Stable oxygen isotope anomaly ($\Delta^{17}O = \delta^{17}O - 0.52 \times \delta^{18}O$) is recognized as a powerful tool to track formation pathways of atmospheric $NO_3^-$. This is because the oxygen atoms in the terminal positions of $O_3$ exhibit an elevated $\Delta^{17}O$ ($\Delta^{17}O = 39 \pm 2‰$), (Vicars and Savarino, 2014) whereas the $\Delta^{17}O$ values of other atmospheric oxidants (e.g., $H_2O$, OH, and $RO_2$) that can be incorporated to $NO_3^-$ are very close to 0‰. (Dubey et al., 1997; Barkan and Luz, 2003; Alexander et al., 2020) Therefore, $\Delta^{17}O(NO_3^-)$ serves as a unique tracer of $O_3$ involvement in its formation pathways, offering valuable insights into the relative contributions of individual reactions. In recent years, the use of $\Delta^{17}O(NO_3^-)$

to elucidate $NO_3^-$ formation has garnered considerable attention. Walters et al. (2024) reported that the major formation pathways of annual $HNO_3$ production in the northeastern U.S. are $NO_2$+OH (46%), $N_2O_5$ uptake (34%), and organic nitrate hydrolysis (12%), with notable seasonal variability. Additionally, Zhang et al. (2022) observed that the contribution of nocturnal chemistry to $NO_3^-$ formation increases at night, peaking at 72% around midnight. In contrast, the contribution of $NO_2$+ OH rises with sunrise, reaching its highest fraction (48%) around noon. However, nearly all current $\Delta^{17}O$-related observations have been conducted in the plain cities, with little attention given to plateau cities, where atmospheric conditions generally suffer from distinct energy consumption patterns and unique climatic factors (e.g., intense solar radiation). In this study, we present detailed results from comprehensive field observations conducted in Lhasa (3650 m a.s.l), one of the highest cities in the world, located on the Tibetan Plateau, China. For the first time, we quantify the relative contribution of three oxidation pathways to $NO_3^-$ formation in Lhasa on the basis of ambient measurements for $\Delta^{17}O$ signatures in $NO_3^-$.

## 2. Materials and methods

### 2.1 Sampling campaign

$PM_{2.5}$ samples were collected on the roof of a building (~15 m above ground) at the Meteorological Bureau of Lhasa (91.08°E, 29.40°N; Figure 1) in China. This site is located in Chengguan, a typical urban area of Lhasa characterized by a dense population and nearby temples. The sampling campaign was conducted from June 2022 to July 2023 using a high-volume $PM_{2.5}$ sampler, which operated at a flow rate of 1.0 $m^3$/min. Samples were collected once a week, with each sampling session lasting 48 hours, except during intensive sampling periods in the summer (June 30 to July 14, 2022) and winter (January 28 to February 7, 2023). During these intensive periods, each sample was collected for 12 hours, from 8:00 to 20:00 and 20:00 to 8:00 on the following day, respectively. Before sampling, all quartz filters (8 in. × 10 in., Pallflex) were calcined in a muffle furnace at 450 °C for 6 h to prevent impurities from contaminating the collected $PM_{2.5}$ samples. After sampling, the samples were collected and stored in a freezer at -20℃.

https://doi.org/10.5194/egusphere-2025-164
Preprint. Discussion started: 7 March 2025

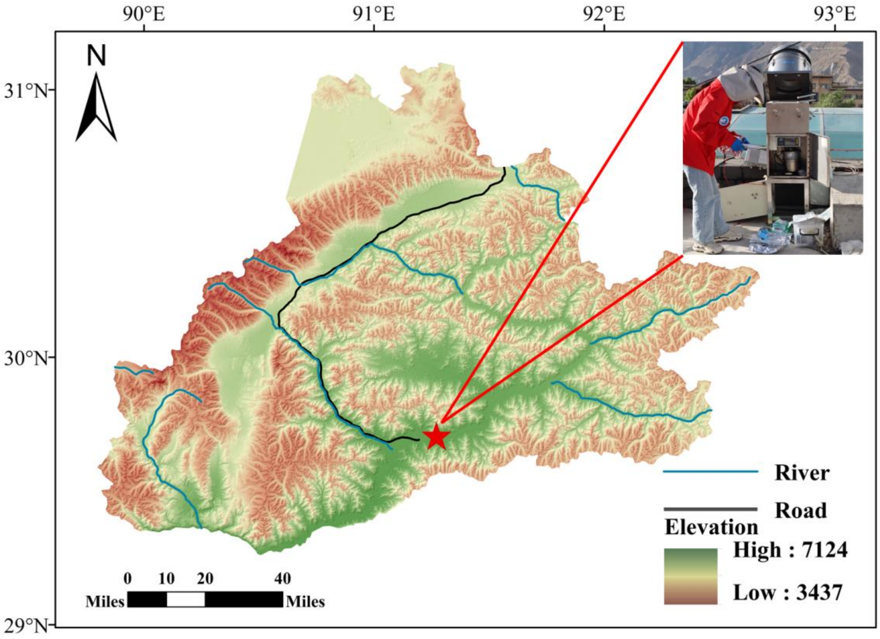

*Figure 1. Geographic position of sampling site in Lhasa, China.*

## 2.2 Measurements of water-soluble ions and isotopes

Water-soluble ions were measured by an ion chromatography (Dionex ICS-5000, Thermo Scientific Inc.) (Chen et al., 2022). In brief, a part of filter membranes (4.54 $cm^2$) was cut using a 17 mm diameter punch and placed in a 15 mL centrifuge tube with 10 mL of 18.2 MΩ ultrapure water. The tube was then subjected to ultrasonic treatment in an ice-water bath for 30 min to prevent ion volatilization. The extract was filtered through a 0.22 μm filter into a 30 mL sample bottle. This process was repeated with an additional 10 mL of water to ensure full extraction. The final extract was analyzed by an ion chromatography. The method detection limit (MDL) of $NO_3^-$ was 0.003 mg/L.

Stable oxygen isotopes ($\delta^{17}O$, $\delta^{18}O$, $\Delta^{17}O$, and $\Delta^{17}O = \delta^{17}O - 0.52 \times \delta^{18}O$) of $NO_3^-$ were determined using an isotope ratio mass spectrometer (MAT253, Thermo Fisher Scientific, USA) at Nanjing University of Information Science and Technology (Fan et al., 2021; Zhang et al., 2022). Briefly, $NO_3^-$ from filter extractions (containing at least 0.8 μg N) was converted into gaseous $N_2O$ using the bacterial denitrifier method. $N_2O$ was then further thermally decomposed into $O_2$ and $N_2$ in a gold tube heated to 800°C. The produced $O_2$ was analyzed for oxygen isotopes by isotope ratio mass spectrometer. The duplicated analysis showed that the errors were within 1.32% for $\Delta^{17}O$-$NO_3^-$.

### 2.3 Primary data sources

Meteorological parameters, including ambient temperature (T), relative humidity (RH), rainfall, radiation, wind direction (WD) and wind speed (WS) during the sampling campaign, were obtained from the Meteorological Bureau of Lhasa. Additionally, $NO_2$ and $O_3$ during the sampling campaign were downloaded from the National Meteorological Information Center (http://air.cnem.cn:18007/).

### 2.4 Stable isotope analysis in the R (SIAR) model

In this study, stable isotope analysis in the R (SIAR) model was employed to estimate the relative contributions of three main pathways to $NO_3^-$ (Parnell et al., 2010). The SIAR model is well-suited for analyzing multiple formation pathways, as it effectively incorporates uncertainties and parameter variability, leading to more reliable estimates. Specifically, this model allows for a detailed analysis of oxygen isotope ($\Delta^{17}O$), enabling accurate modeling of $NO_3^-$ formation pathways based on oxygen isotope measurements. The SIAR model is a Bayesian mixture model, mathematically formulated as follows:

$$X_i = \sum_{j=1}^{K} p_j \times f_{ij}$$

$$p_1 + p_2 + \cdots + p_k = 1$$

$$f_{ij} \sim N\left(\mu_j, \omega_j^2\right)$$

Where $X_i$ is the observed $\Delta^{17}O$ values for sample *i* ($i = 1, 2, 3, \ldots$,N) and $p_j$ is the proportional contribution of each $NO_3^-$ formation pathway *j* to the sample *i*. $f_{ij}$ is the $\Delta^{17}O$ values of formation pathway *j* for sample *i* and follows a normal distribution with mean ($\mu_j$) and variance ($\omega_j^2$). Within the Bayesian framework, prior distributions are assigned to each $p_j$, and these are updated with the observed data $X_i$ to obtain posterior distributions, allowing for inference of the proportional contributions $p_j$ of each pathway.

### 2.5 Aerosol liquid water content (ALWC) and the Hybrid Single-Particle Lagrangian Integrated Trajectory (HYSPLIT)

To evaluate the influence of aerosol liquid water content (ALWC) on the $NO_3^-$ formation, ALWC was calculated using the ISORROPIA II model developed by Fountoukis and Nenes (Fountoukis and Nenes, 2007). The ISORROPIA II model includes two modes: the forward mode, which requires the concentrations of both particulate and gaseous pollutants concentrations as inputs, and the reverse

https://doi.org/10.5194/egusphere-2025-164
Preprint. Discussion started: 7 March 2025

mode, which only requires the concentrations of particulate pollutants concentrations. The model computes the ALWC in both modes based on particulate pollutant concentrations (e.g., $NH_4^+$, $Na^+$, $Ca^{2+}$, $K^+$ and $Mg^{2+}$), as well as ambient RH and T. In this study, the reverse mode was employed due to the lack of gaseous pollutant concentrations observations.

Additionally, the Hybrid Single-Particle Lagrangian Integrated Trajectory (HYSPLIT) model was utilized to compute 72-hours back trajectories during the sampling campaign. HYSPLIT, developed by the National Oceanic and Atmospheric Administration Air Resources Laboratory (NOAA/ARL), is available on the their website (http://www.arl.noaa.gov/ready/hysplit4.html), This model has been widely used for simulating the transport and dispersion trajectories of pollutants such as $PM_{2.5}$, $VOC_s$, $O_3$, and $NO_x$, among others. Backward trajectories for each sampling day were calculated at an altitude of 3650 meters using meteorological data from the Global Data Assimilation System (GDAS), available through the US Air Resources Laboratory (NOAA ARL) (https://www.ready.noaa.gov/data/archives/gdas1/).

# 3. Results

## 3.1 Overview of the meteorological parameters in Lhasa during the sampling campaign

Figure 2a presents the daily variations in meteorological parameters, including temperature, relative humidity (RH), rainfall and solar radiation. During the sampling campaign, the annual average temperature was 11.5°C, ranging from -2.83 to 24.2°C. The highest average temperature was observed in summer (19.7°C), while the lowest (3.11°C) was recorded in winter. Relative humidity (RH) varied between 6.67 and 66.8%, with the lowest average RH occurring in winter (17.1%) and the highest in summer (35.6%). The near-surface layer of Lhasa is influenced by a thermal low-pressure system, and the southwest monsoon, active between June and September, transports moisture-laden air from the Indian Ocean, resulting in increased rainfall during summer. Solar radiation intensity exhibited a seasonal trend opposite to those of temperature and RH, peaking in summer (394 W/m$^2$) and reaching its lowest levels in winter (220 W/m$^2$). The dominant wind direct (WD) was southeast in spring, but southwest in the other three seasons (Figure 3). Wind speed (WS) was highest in spring but lowest in autumn.

## 3.2 $NO_3^-$ concentration

$NO_3^-$ mass concentrations ranged from 0.10 to 1.72 μg/m$^3$, with an average value of 0.62 ± 0.31 μg/m$^3$. $NO_3^-$ concentrations exhibited distinct seasonal patterns. Specifically, the maximum monthly average values of $NO_3^-$ concentration occurred in spring (0.83 ± 0.35 μg/m$^3$) with the instantaneous maximum reaching 1.72 μg/m$^3$, whereas the lowest was recorded in autumn (0.23 ± 0.13 μg/m$^3$) with an instantaneous minimum of only 0.09 μg/m$^3$ (Table 1). The difference in $NO_3^-$ concentrations between autumn and other three seasons was statistically significant ($p < 0.05$). The considerable seasonal variation in $NO_3^-$ concentrations in Lhasa is associated with varying emission sources and meteorological conditions. In spring, high $NO_3^-$ concentrations were associated with weak southeasterly winds (< 3 m/s) in the bivariate polar plot, suggesting probable impacts from local/regional emissions (Figure 3). During the rainy summer, shorter $NO_3^-$ lifetimes indicate a weak influence from regional transport, with a more pronounced contribution from local/regional emissions. In autumn, $NO_3^-$ concentrations were relatively low, partly due to the reduced local emissions caused by the COVID-19 pandemic, which led to decreased human activity and transportation. Despite low wind speed, the lower $NO_3^-$ levels during this period suggest that the pandemic, combined with seasonal meteorological conditions, played a role in limiting local/regional emissions. In winter, elevated $NO_3^-$ concentrations under low wind speeds (< 3 m/s) emphasize the significant contribution of local/regional emissions. These findings underscore that, in addition to regional transport, local emissions are the primary contributor to $NO_3^-$ concentrations in Lhasa, especially under low wind conditions, with the pandemic further influencing local emission levels. Furthermore, based on our day-night sampling scheme, no nychthemeral (day-night) differences in $NO_3^-$ concentrations were detected (Table S1). A similar day-night pattern of $NO_3^-$ concentrations also has been observed in in Beijing (Luo et al., 2020).

Table 1 Average values of water-soluble ions and $\Delta^{17}O$-$NO_3^-$ during the sampling campaign

| | | $Na^+$ µg/m$^3$ | $NH_4^+$ µg/m$^3$ | $K^+$ µg/m$^3$ | $Mg^{2+}$ µg/m$^3$ | $Ca^{2+}$ µg/m$^3$ | $Cl^-$ µg/m$^3$ | $NO_3^-$ µg/m$^3$ | $SO_4^{2-}$ µg/m$^3$ | $\Delta^{17}O$-$NO_3$- ‰ |
|---|---|---|---|---|---|---|---|---|---|---|
| **Annual** | **Minmum** | 0.02 | 0 | 0.004 | 0.004 | 0.004 | 0.004 | 0.09 | 0.06 | 18.3 |
| | **Maximum** | 0.68 | 1.22 | 0.29 | 0.08 | 3.52 | 0.51 | 1.72 | 2.37 | 34.1 |
| | **Average** | 0.16 | 0.3 | 0.07 | 0.02 | 1.09 | 0.08 | 0.62 | 0.74 | 26.3 |
| | **Std.Dev** | 0.14 | 0.26 | 0.06 | 0.01 | 0.7 | 0.1 | 0.31 | 0.45 | 3.13 |
| **spring** | **Minmum** | 0.04 | 0.16 | 0.04 | 0.01 | 1.02 | 0.01 | 0.45 | 0.6 | 27.2 |
| | **Maximum** | 0.16 | 1.22 | 0.2 | 0.05 | 2.56 | 0.05 | 1.72 | 2.14 | 30.4 |
| | **Average** | 0.09 | 0.52 | 0.09 | 0.02 | 1.67 | 0.03 | 0.83 | 1.11 | 28.8 |
| | **Std.Dev** | 0.03 | 0.3 | 0.04 | 0.01 | 0.51 | 0.01 | 0.35 | 0.52 | 0.99 |
| **summer** | **Minmum** | 0.02 | 0 | 0.01 | 0.01 | 0.03 | 0.003 | 0.13 | 0.18 | 20.2 |
| | **Maximum** | 0.4 | 1.08 | 0.09 | 0.04 | 2.4 | 0.13 | 1 | 2.37 | 28.5 |
| | **Average** | 0.09 | 0.18 | 0.03 | 0.02 | 1.15 | 0.3 | 0.5 | 0.72 | 25.5 |
| | **Std.Dev** | 0.08 | 0.17 | 0.02 | 0.01 | 0.5 | 0.3 | 0.23 | 0.45 | 2.2 |
| **autumn** | **Minmum** | 0.02 | 0.003 | 0.004 | 0.01 | 0.004 | 0.01 | 0.09 | 0.06 | 21.2 |
| | **Maximum** | 0.17 | 0.11 | 0.1 | 0.03 | 0.24 | 0.17 | 0.51 | 0.55 | 24.9 |
| | **Average** | 0.09 | 0.04 | 0.3 | 0.02 | 0.13 | 0.05 | 0.23 | 0.31 | 23.05 |
| | **Std.Dev** | 0.05 | 0.04 | 0.3 | 0.01 | 0.08 | 0.05 | 0.13 | 0.14 | 1.44 |
| **winter** | **Minmum** | 0.06 | 0.09 | 0.02 | 0.01 | 0.05 | 0.04 | 0.21 | 0.32 | 18.3 |
| | **Maximum** | 0.56 | 0.87 | 0.29 | 0.08 | 3.52 | 0.51 | 1.46 | 1.57 | 34.1 |
| | **Average** | 0.19 | 0.44 | 0.12 | 0.03 | 1.04 | 0.16 | 0.75 | 0.73 | 25.9 |
| | **Std.Dev** | 0.12 | 0.21 | 0.08 | 0.02 | 0.78 | 0.13 | 0.28 | 0.34 | 3.86 |

https://doi.org/10.5194/egusphere-2025-164
Preprint. Discussion started: 7 March 2025

### 3.3 Oxygen isotopes of $NO_3^-$

To explore the three major oxidation pathways of $NO_3^-$ formation, 53 samples representing varying $NO_3^-$ concentrations across different seasons were selected for oxygen isotope measurements. The $\Delta^{17}O$-$NO_3^-$ values ranged from 18.3 to 34.1‰, with an average of 26.3 ± 3.13‰, which is slightly lower than the global average of 28.6 ± 4.5‰ simulated by the Global Chemical Transport Model (Alexander et al., 2020). As shown in Table S3, the observed $\Delta^{17}O$-$NO_3^-$ values in this study were similar to most mid- and low-latitude regions, but lower than those in polar regions (~ 32‰). Clear seasonal variations in $\Delta^{17}O$-$NO_3^-$ values were seen in Lhasa (Figure 2b). As listed in Table S1, the average $\Delta^{17}O$-$NO_3^-$ values in spring, summer, autumn and winter were 28.8 ± 8.0‰, 25.5 ± 2.20‰, 25.6 ± 1.35‰, and 25.9 ± 3.56‰, respectively. The differences in $\Delta^{17}O$-$NO_3^-$ values between spring and summer, as well as between spring and winter, were statistically significant ($p < 0.05$). The elevated $\Delta^{17}O$-$NO_3^-$ values in spring could be attributed to a higher proportion of nocturnal pathways that enrich $\Delta^{17}O$-$NO_3^-$ values, such as $NO_3$ + VOC and $N_2O_5 + H_2O$ pathway. In contrast, the lower $\Delta^{17}O$-$NO_3^-$ values in other three seasons suggested a greater production of $NO_3^-$ formation via $NO_2$ + OH pathway, leading to more negative $\Delta^{17}O$-$NO_3^-$ values. Diurnal variation in $\Delta^{17}O$-$NO_3^-$ values also differed across season. In summer, the average of $\Delta^{17}O$-$NO_3^-$ values during the day (25.3 ± 2.39‰) was lower than at night (26.7 ± 1.03‰). Conversely, in winter, the average of $\Delta^{17}O$-$NO_3^-$ values during the day (28.0 ± 3.79‰) was significantly higher than at the night (24.4 ± 3.85‰). Similar diurnal patterns, with higher daytime $\Delta^{17}O$-$NO_3^-$values and lower nighttime values, have also been observed in winter in the U.S. (Vicars et al., 2013) and other cities in China (He et al., 2018).

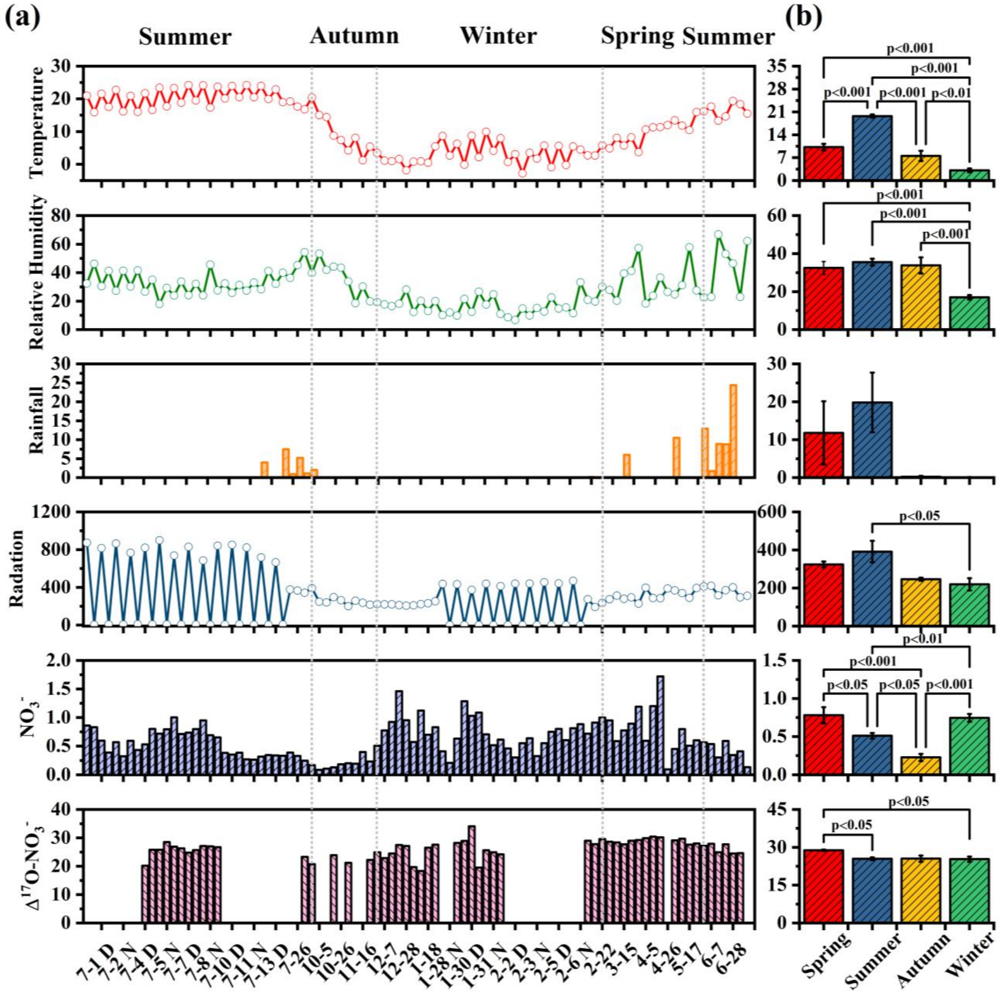

*Figure 2. (a) shows the time series of temperature (℃), relative humidity (%), Rainfall (mm), Radiation (W/m$^2$), $NO_3^-$ concentration (μg/m$^3$), and $\Delta^{17}O$- $NO_3^-$ (‰) from June 30 2022 to July, 2023. (b) shows the average values significance at different seasons with their statistical.*

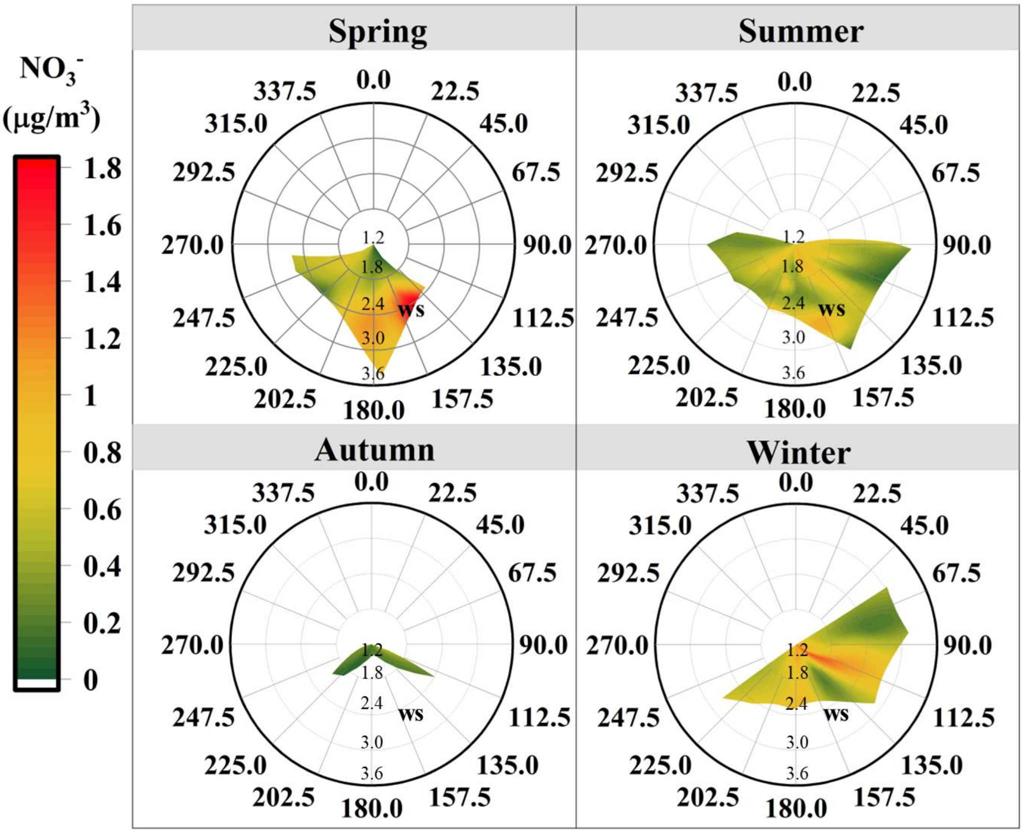

*Figure 3. Bivariate polar plot illustrates the seasonal variation in the mass concentration of* $NO_3^-$ *in relation to wind speed (WS, m/s) and wind direction (WD, degrees).*

# 4. Discussion

## 4.1 A comparison of $NO_3^-$ oxidation pathways in Lhasa with other megacities in plain regions

Typically, observations of $\Delta^{17}O$-$NO_3^-$ and estimated α (the proportion of $O_3$ oxidation in $NO_2$ production rate) values are employed to quantify the contributions of major $NO_3^-$ oxidation pathway in conjunction with a Bayesian model. The α value ranged from 0.63 to 0.93, with an average of 0.83 ± 0.06, suggesting the significance of $O_3$ participation in NO oxidation during the sampling campaign. On the other hand, our α values were lower than those (0.85-1) for other midlatitude regions, likely due to stronger UV radiation enhancing OH radical production and competitive oxidation pathways involving VOC and $RO_2$ in Lhasa. On average, the relative contributions of $NO_2$ + OH ($f_{NO2+OH}$), $NO_3$

+ VOC ($f_{NO3+VOC}$) and $N_2O_5$ + $H_2O$ ($f_{N2O5+H2O}$) to $NO_3^-$ formation in Lhasa during the sampling campaign were 46 ± 26%, 26 ± 19% and 28 ± 11%, respectively. To better understand the characteristics of $NO_3^-$ formation mechanism in Lhasa, we performed a detailed comparison around the China for the relative contributions of key oxidation pathways using the $\Delta^{17}O$ methodology (Figure 4). Overall, similar to most Chinese cities, $NO_3^-$ formation in Lhasa was predominantly driven by the $NO_2$ + OH pathway, exhibiting distinct seasonal and regional variations. In particular, the average $f_{NO3+VOC}$ values were generally several times higher in spring in Lhasa than in other urban cities. Compared to rural/remote areas, the average $f_{NO3+VOC}$ values showed higher fractions in Lhasa, reveling the influence of anthropogenic emission, i.e., vehicle exhaust and heating, on $NO_3^-$ formation. In Lhasa, the Capital of Tibet, field measurements among different years showed a substantial increase in VOC concentrations in urban areas of the Tibet Plateau, comparable to those in North China (Tang et al., 2022), revealing the importance of the active $NO_3$ + VOC pathway for $NO_3^-$ pollution formation in Lhasa. Recent studies have emphasized that $NO_3$ + VOC is a major formation mechanism of $NO_3^-$ production. For instance, Fan et al. (2021) used $\Delta^{17}O$-$NO_3^-$ to reveal that the average $f_{NO3+VOC}$ value was 17% in summer and increased to 32% in winter based on $\Delta^{17}O$-$NO_3^-$ observations in Beijing. He et al. (2018) estimated the relative contributions of $NO_3$ + VOC and $N_2O_5$ + $Cl^-$ to $NO_3^-$ formation and found that $NO_3$ + VOC and $N_2O_5$ + $Cl^-$ were in the range of 16-56%, underscoring the significant roles of these pathways during haze events in Beijing. Meanwhile, Feng et al. (2023) also reported that the $f_{NO3+VOC}$ values were up to 49.6% in winter in northern China. Additionally, Wang et al. (2023) noted that in Guangzhou, the average $f_{NO3+VOC}$ value was at the 488m (25%) higher than that at the ground (12%). Li et al. (2022) utilized $\Delta^{17}O$-$NO_3^-$ to explore the oxidation pathway of $NO_3^-$ in both urban and rural atmosphere in Northeast China and found that the $f_{NO3+VOC}$ values increased from 5% in urban areas to 13.5% in rural areas.

https://doi.org/10.5194/egusphere-2025-164
Preprint. Discussion started: 7 March 2025

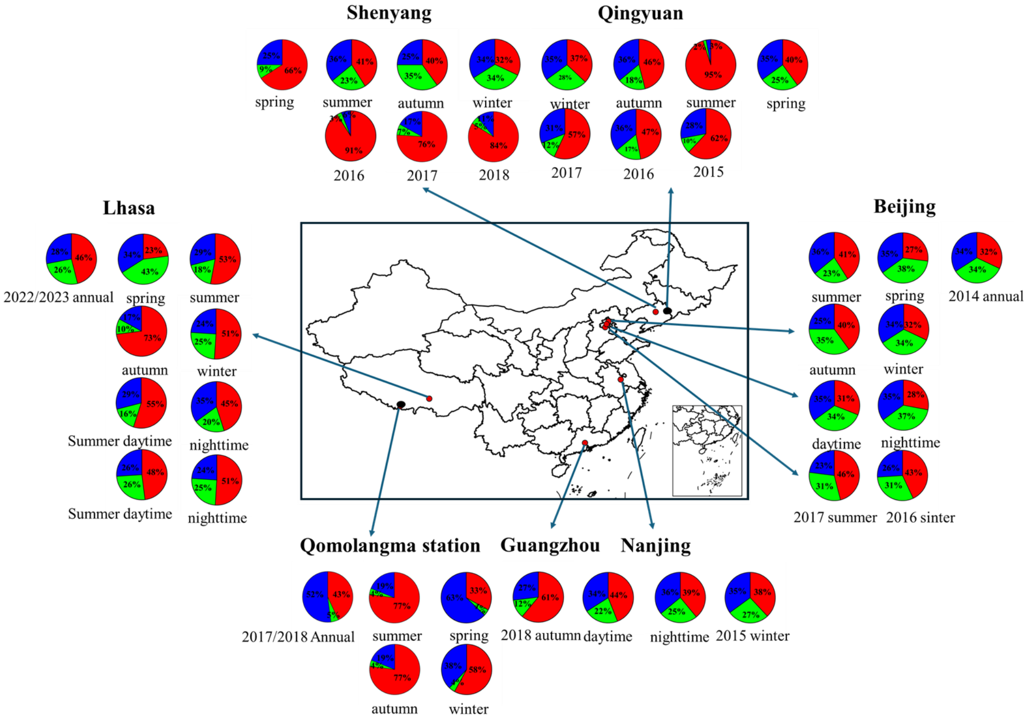

*Figure 4. Summary of the relative contributions of key oxidation pathways using the $\Delta^{17}O$ methodology around the China (data given in Table S3 in the Supplement). Colors for the study labels indicate the type of sampling location: urban areas (red), and rural/remote areas (black). The pie charts show the relative contribution of different pathways to $NO_3^-$ formation: $f_{NO2+OH}$ (red), $f_{NO3+VOC}$ (green), and $f_{N2O5+H2O}$ (blue).*

### 4.2 Seasonal and diurnal variations of $NO_3^-$ oxidation pathways

Figure S1 illustrates the seasonal variations in the relative contributions of the three main oxidation pathways to $NO_3^-$ formation. When comparing different seasons, the $f_{NO2+OH}$ values were lower ($p < 0.01$) in spring (22.6%) than in winter (50.8%), summer (52.9%) and autumn (73.2%). The $NO_2$ concentration was 12.7 ± 1.81 $\mu g/m^3$ in spring, which was higher than in autumn (11.3 ± 5.83 $\mu g/m^3$). Therefore, the reduced $f_{NO2+OH}$ in spring cannot be attributed to lower $NO_2$ levels. Typically, high solar radiation enhances $NO_3^-$ formation via the $NO_2$ + OH pathway. However, this pathway has been shown to be suppressed in clean atmospheric conditions with low particulate matter loadings (Zhang et al., 2022; Fan et al., 2021). The mean $NO_3^-$ concentration was higher in spring (0.83 ± 0.35 $\mu g/m^3$) compared to autumn (0.23 ± 0.13 $\mu g/m^3$), which might account for the higher $f_{NO2+OH}$ in autumn.

A significant increase in the $f_{NO3+VOC}$ values was observed in spring ($p < 0.05$). First, $O_3$ and $NO_2$

are precursors of $NO_3$. In this work, highest concentrations of $O_3$ were found in spring (114.9 ± 18.1 μg/m$^3$), likely leading to elevated $NO_3$ concentrations. The low temperature and reduced OH concentrations in spring facilitate the reaction of $NO_2$ and $O_3$ to synthesize $NO_3$. This might be an appropriate reason for the $f_{NO3+VOC}$ values in spring. Second, previous study has indicated that the Afghanistan-Pakistan-Tajikistan region, the Indo-Gangetic Plain, and Meghalaya-Myanmar region could transport industrial VOC to various zones in Tibet from west to east. Additionally, agricultural areas in northern India could contribute biomass burning-related VOC to the middle-northern and eastern regions of Tibet (Li et al., 2017). The W and S air clusters were notably prevalent in the springtime, coinciding with intensive fire spots observed in Afghanistan, Pakistan, India, Nepal, and Bhutan (Figure S2/S3). Air masses originating from and traversing these regions are likely to pick up VOC emitted from biomass burning and transport them to the sampling site, thereby enhancing the $f_{NO3+VOC}$ values in spring.

Similarly, the $f_{N2O5+H2O}$ values exhibited its highest contributions during spring, with significant seasonal differences ($p < 0.05$) except when compared to summer ($p > 0.05$). Typically, high RH enhances $NO_3^-$ formation via $N_2O_5 + H_2O$ pathway. However, studies have revealed that during sandstorm events, a significant large $N_2O_5$ uptake coefficient is observed on urban aerosols in spring (Xia et al., 2019). In this study, the mean $Ca^{2+}$ concentration in $PM_{2.5}$ was found to be the highest in spring, suggesting a possible role of dust in facilitating $N_2O_5$ uptake. Additionally, $N_2O_5 + H_2O$ pathway has been reported to be promoted by elevated $NO_3^-$ concentrations, (Lin et al., 2021) which were also highest in spring. Therefore, the increased $f_{N2O5+H2O}$ values during spring might be attributed to the combined effects of lower RH, elevated $Ca^{2+}$ levels, and high $NO_3^-$ concentrations.

Interestingly, distinct diurnal patterns of $NO_3^-$ oxidation pathways were observed during the sampling campaign (Figure 5). In summer, $NO_2$ + OH pathway showed a significantly higher contribution during the daytime (55.1%) compared to nighttime (44.9%), which is attributed to increased OH radical synthesis during longer days and higher temperatures in Lhasa (Rohrer and Berresheim, 2006). A previous study indicated that lower $NO_2$ and higher $O_3$ concentrations enhance the relative contribution of OH pathway to $NO_3^-$ formation (Wang et al., 2019). Additionally, the concentration of aerosol liquid water content (ALWC, the detailed information is given in Text S3) was higher at night than during the day in summer, favoring $NO_3^-$ formation through nocturnal formation. In winter, $f_{NO2+OH}$, $f_{NO3+VOC}$ and $f_{N2O5+H2O}$ were similar during both day and night. Typically, daytime $NO_3$ and $N_2O_5$ chemistry is considered less important due to rapid photolysis of $NO_3$ and the titration reaction initiated by NO. However, Wang et al. (2020) demonstrated that the daytime production rate of $NO_3$ can be substantial due to increased concentrations of $NO_2$ and $O_3$ in winter. Although $NO_3$ titration occurs rapidly and the atmospheric lifetimes of $NO_3$ and $N_2O_5$ are short, their daytime concentrations are not negligible. A recent study found that in winter, the amount of $NO_3$ radical during the day was comparable to that at night, whereas in summer, daytime $NO_3$ radicals were lower than those at night (Brown et al., 2011). This discrepancy in $NO_3$ radical levels might explain the differences in $NO_3^-$ formation pathways between summer and winter. Furthermore, in winter, lower temperatures and elevated $NO_2$ concentrations facilitate a quasi-steady-state equilibrium between $NO_3$ and $N_2O_5$, slowing the overall reactivity of the $NO_3^-$ precursors. This equilibrium condition minimizes diurnal fluctuations in precursor concentrations, resulting in relatively stable nocturnal and daytime $NO_3^-$ formation pathways, including $NO_3$ + VOC and $N_2O_5 + H_2O$. Consequently, under such equilibrium conditions, the $NO_2$ + OH pathway remains comparatively steady between day and night, as OH generation is limited. Conversely, in summer, elevated temperatures and extended photoperiod prevent $NO_3$ and $N_2O_5$ from achieving steady-state equilibrium, leading to greater variability in $NO_3^-$ formation. Thus, $NO_3^-$ production becomes more sensitive to photochemical and VOC fluctuations, resulting in a pronounced contrast between daytime and nighttime $NO_3^-$ formation pathways (Brown et al., 2003).

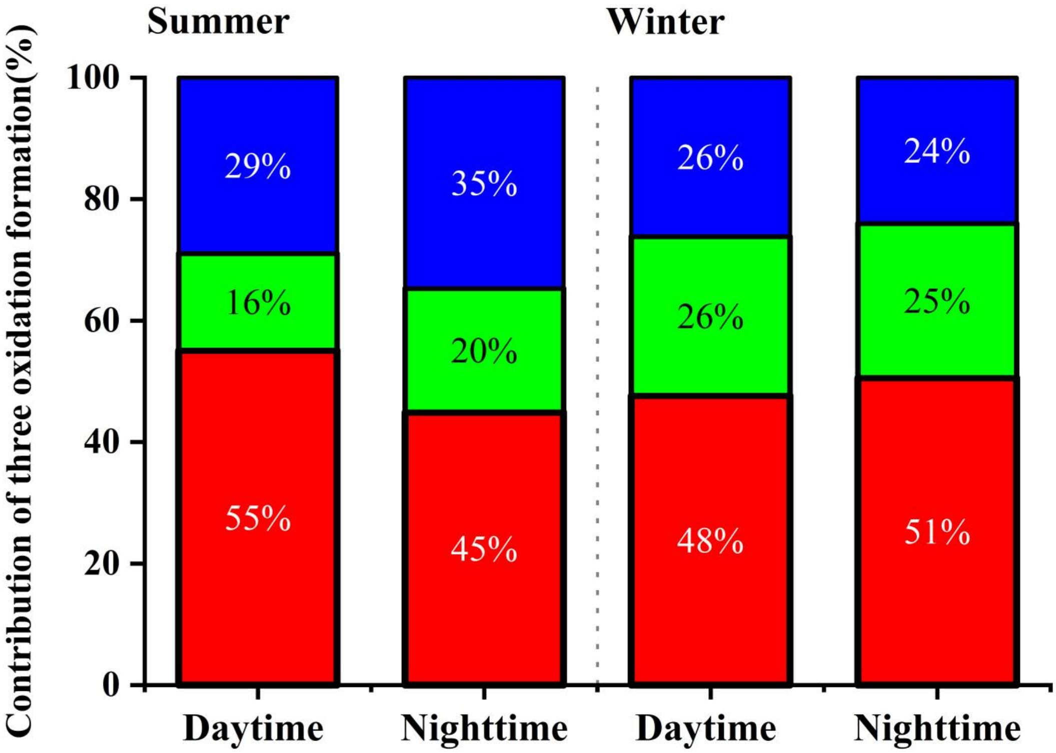

*Figure 5. the relative contributions of $NO_2$+OH, $NO_3$+VOC, and $N_2O_5$+$H_2O$ to $NO_3^-$ formation during the day and night in summer and winter in Lhasa during the sampling campaign. The contributions are represented as $f_{NO2+OH}$ (red), $f_{NO3+VOC}$ (green), and $f_{N2O5+H2O}$ (blue).*

### 4.3 Integrated analysis of $NO_3^-$ oxidation pathways in Lhasa

As shown in Figure S4, $NO_3$ + VOC pathway emerged as the major contributor to $NO_3^-$ formation during periods of high $NO_3^-$ spikes. To elucidate the mechanisms driving $NO_3^-$ formation under varying conditions, $NO_3^-$ samples were categorized into different concentration ranges (Figure 6). We found the $f_{NO3+VOC}$ values increased and $f_{NO2+OH}$ values decreased with the $NO_3^-$ concentrations. This significant decrease in $f_{NO2+OH}$ values in the air pollution is predictable, as OH radical production tends to decline with increasing air pollution, especially on heavily polluted and hazy days (Bäumer et al., 2008). In addition to concentration effects, meteorological factors typically also regulate the $NO_3^-$ oxidation pathways. Typically, high temperature promotes the $NO_3^-$ formation in $f_{NO2+OH}$ values (Han et al., 2015). However, our study revealed that the relationship between temperature and $f_{NO2+OH}$ values did not consistently show a positive trend. Further analysis indicated that $NO_2$ and $O_3$ concentrations were negatively correlated, with lower $NO_2$ concentrations paired with elevated $O_3$ levels (Figure S5).

$f_{NO2+OH}$ values reached its minimum when $NO_2$ was between 15 and 20 μg/m$^3$ and $O_3$ was within 100-120 μg/m$^3$. Although OH radicals exhibit a higher oxidation potential (2.8 V) than $O_3$ (2.07 V), but atmospheric availability is much lower than that of $O_3$ (Carslaw et al., 1999; Dubey et al., 1997). Therefore, $NO_2$ at lower concentrations is more likely to be oxidized by OH than by $O_3$, even though $O_3$ concentrations were high. With increasing $NO_2$ concentrations, the availability of OH radicals for oxidating $NO_2$ became lower, resulting in a relatively higher proportion of $NO_2$ being oxidized by $O_3$ although $O_3$ concentrations were low. However, when the concentration of $O_3$ is below 20 μg/m$^3$, $O_3$ concentrations were not sufficient to oxidize $NO_2$ due to the higher $NO_2$ concentrations and OH radicals for oxidating $NO_2$ would re-dominate. These observations underscore that in high-altitude urban environments like Lhasa, OH effectiveness is more important on $NO_3^-$ oxidation pathways than that of $O_3$. Additionally, we identified an intriguing positive correlation between the atmospheric oxidizing capacity ($O_x = NO_2 + O_3$) and $f_{NO3+VOC}$ values. $f_{NO3+VOC}$ values were lowest when $O_x$ was less than 90 μg/m$^3$, corresponding to a maximum contribution from the $NO_2$ + OH pathway. This suggests that $O_x$ is more indicative of the pathways of $NO_3^-$ formation in the atmosphere compared to either $NO_2$ or $O_3$ alone. Typically, High RH and ALWC were also positively correlated with $f_{N2O5+H2O}$. But RH was associated with variable contributions from the $N_2O_5$+$H_2O$ pathway in our study, while increasing ALWC significantly enhanced this pathway, indicating ALWC as a more reliable indicator of $NO_3^-$ formation.

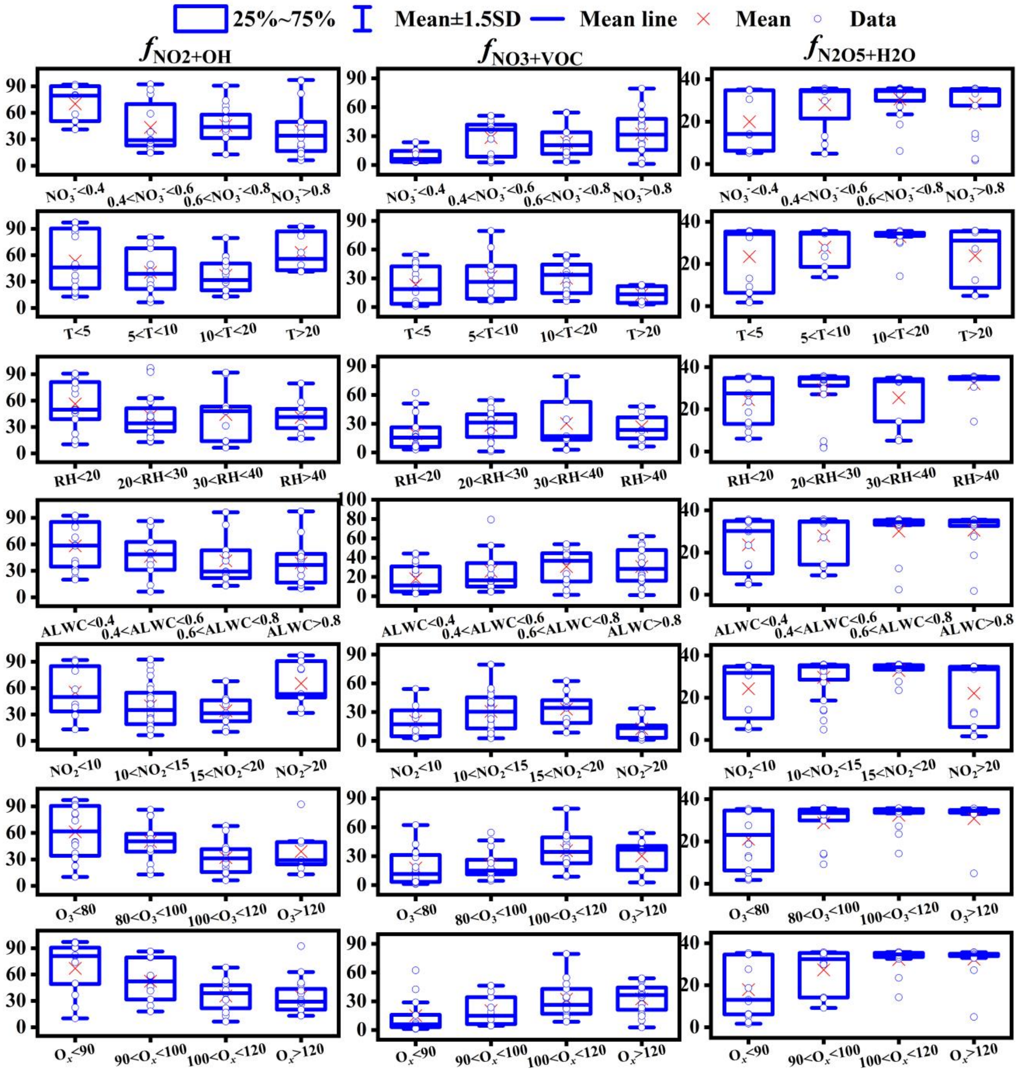

*Figure 6 Influence of $NO_3^-$ (μg/m$^3$), temperature (℃), RH (%), ALWC (μg/m$^3$), $NO_2$ (μg/m$^3$), $O_3$ and $O_x$(μg/m$^3$) on $NO_3^-$ formation pathways (%).*

## 4.4 Implications

The oxidation pathways of $NO_3^-$ in Lhasa, China, were constrained using a full year of $\Delta^{17}O$-$NO_3^-$ measurements from 2022 to 2023. Based on seasonal data, we observed a significant increase in the relative contribution of the $NO_3$+VOC to $NO_3^-$ formation during the spring. Furthermore, the diurnal distribution of $NO_3^-$ oxidation pathways varied distinctly across seasons. To better understand the factors influencing these pathways, we integrated meteorological conditions, NO*x* precursors, and

ALWC for a more comprehensive analysis of $NO_3^-$ formation. The results revealed that O*x* and ALWC are more reliable indicators of $NO_3^-$ oxidation pathways than meteorological factors. Atmospheric ALWC is primarily produced by hygroscopic aerosols such as $SO_4^{2-}$, $NH_4^+$, and $Cl^-$. Therefore, in addition to controlling $NO_2$, $O_3$, and VOC, reducing these hygroscopic aerosols is crucial for effective $PM_{2.5}$ pollution control.

## Data availability

All data are presented in the main text and/ or the Supplement. For additional data, please contact the corresponding author (liu.junwen@jnu.edu.cn).

## Author contributors

JL designed, conceived, and led the research. XZ performed the data analysis and drafted the manuscript. JL, XZ NC and BB planned and carried out the measurements. NC, BB and PD were responsible for measuring the meteorological parameters. JL and PY secured funding for the continuous aerosol sampling and analysis. FC and YZ provided expertise on isotope analysis methods. JL offered guidance on data analysis, and all authors contributed to revising the manuscript.

## Competing interests

The authors declare no competing financial interest.

## Acknowledgments

This study was supported by the Natural Science Foundation of Xizang Autonomous Region (XZ202401ZR0067), Guangdong Basic and Applied Basic Research Foundation (2024B1515040026) and the second Tibetan Plateau Scientific Expedition and Research Program (20190ZKK0604).

# Reference

Alexander, B., Sherwen, T., Holmes, C. D., Fisher, J. A., Chen, Q., Evans, M. J., and Kasibhatla, P.: Global inorganic nitrate production mechanisms: comparison of a global model with nitrate isotope observations, Atmospheric Chemistry and Physics, 20, 3859-3877, 2020.

Barkan, E. and Luz, B.: High-precision measurements of $^{17}O/^{16}O$ and $^{18}O/^{16}O$ of $O_2$ and $O_2$/Ar ratio in air, Rapid communications in mass spectrometry, 17, 2809-2814, 2003.

Bäumer, D., Vogel, B., Versick, S., Rinke, R., Möhler, O., and Schnaiter, M.: Relationship of visibility, aerosol optical thickness and aerosol size distribution in an ageing air mass over South-West Germany, Atmospheric Environment, 42, 989-998, 2008.

Bell, M. L., Dominici, F., Ebisu, K., Zeger, S. L., and Samet, J. M.: Spatial and temporal variation in $PM_{2.5}$ chemical composition in the United States for health effects studies, Environmental health perspectives, 115, 989-995, 2007.

Brown, S. S., Stark, H., and Ravishankara, A.: Applicability of the steady state approximation to the interpretation of atmospheric observations of $NO_3$ and $N_2O_5$, Journal of Geophysical Research: Atmospheres, 108, 2003.

Brown, S. S., Dubé, W. P., Peischl, J., Ryerson, T. B., Atlas, E., Warneke, C., de Gouw, J. A., te Lintel Hekkert, S., Brock, C. A., and Flocke, F.: Budgets for nocturnal VOC oxidation by nitrate radicals aloft during the 2006 Texas Air Quality Study, Journal of Geophysical Research: Atmospheres, 116, 2011.

Carslaw, N., Creasey, D. J., Heard, D. E., Lewis, A. C., McQuaid, J. B., Pilling, M. J., Monks, P. S., Bandy, B. J., and Penkett, S. A.: Modeling OH, $HO_2$, and $RO_2$ radicals in the marine boundary layer: 1. Model construction and comparison with field measurements, Journal of Geophysical Research: Atmospheres, 104, 30241-30255, https://doi.org/10.1029/1999JD900783, 1999.

Chen, Z., Pei, C., Liu, J., Zhang, X., Ding, P., Dang, L., Zong, Z., Jiang, F., Wu, L., and Sun, X.: Non-agricultural source dominates the ammonium aerosol in the largest city of South China based on the vertical $\delta^{15}N$ measurements, Science of The Total Environment, 848, 157750, 2022.

Clark, C. M. and Tilman, D.: Loss of plant species after chronic low-level nitrogen deposition to prairie grasslands, Nature, 451, 712-715, 2008.

Colmer, J., Hardman, I., Shimshack, J., and Voorheis, J.: Disparities in $PM_{2.5}$ air pollution in the United States, Science, 369, 575-578, 2020.

Dubey, M. K., Mohrschladt, R., Donahue, N. M., and Anderson, J. G.: Isotope specific kinetics of hydroxyl radical (OH) with water ($H_2O$): Testing models of reactivity and atmospheric fractionation, The Journal of Physical Chemistry A, 101, 1494-1500, 1997.

Espina-Martin, P., Perdrix, E., Alleman, L., and Coddeville, P.: Origins of the seasonal variability of $PM_{2.5}$ sources in a rural site in Northern France, Atmospheric Environment, 120660, 2024.

Fan, M.-Y., Zhang, Y.-L., Lin, Y.-C., Hong, Y., Zhao, Z.-Y., Xie, F., Du, W., Cao, F., Sun, Y., and Fu, P.: Important role of $NO_3$ radical to nitrate formation aloft in urban Beijing: Insights from triple oxygen isotopes measured at the tower, Environmental Science & Technology, 56, 6870-6879, 2021.

Feng, X., Chen, Y., Chen, S., Peng, Y., Liu, Z., Jiang, M., Feng, Y., Wang, L., Li, L., and Chen, J.: Dominant Contribution of $NO_3$ Radical to $NO_3^-$ Formation during Heavy Haze Episodes: Insights from High-Time Resolution of Dual Isotopes $\Delta^{17}O$ and $\delta^{18}O$, Environmental Science & Technology, 57, 20726-20735, 2023.

Ge, S., Su, J., Zhao, P., Li, J., Liu, S., Qiu, Y., Pu, W., and Ma, Z.: Characteristics of $PM_{2.5}$ hygroscopicity and the influences of water-soluble ions during haze events in Beijing, Atmospheric Environment, 322, 120382, https://doi.org/10.1016/j.atmosenv.2024.120382, 2024.

Geng, G., Zheng, Y., Zhang, Q., Xue, T., Zhao, H., Tong, D., Zheng, B., Li, M., Liu, F., and Hong, C.: Drivers of $PM_{2.5}$ air pollution deaths in China 2002–2017, Nature Geoscience, 14, 645-650, 2021.

Han, T., Liu, X., Zhang, Y., Qu, Y., Zeng, L., Hu, M., and Zhu, T.: Role of secondary aerosols in haze formation in summer in the Megacity Beijing, Journal of environmental sciences, 31, 51-60, 2015.

He, P., Xie, Z., Chi, X., Yu, X., Fan, S., Kang, H., Liu, C., and Zhan, H.: Atmospheric $\Delta^{17}O(NO_3^-)$ reveals nocturnal chemistry dominates nitrate production in Beijing haze, Atmospheric Chemistry and Physics, 18, 14465-14476, 2018.

Huang, R.-J., Zhang, Y., Bozzetti, C., Ho, K.-F., Cao, J.-J., Han, Y., Daellenbach, K. R., Slowik, J. G., Platt, S. M., and Canonaco, F.: High secondary aerosol contribution to particulate pollution during haze events in China, Nature, 514, 218-222, 2014.

Li, H., He, Q., Song, Q., Chen, L., Song, Y., Wang, Y., Lin, K., Xu, Z., and Shao, M.: Diagnosing Tibetan pollutant sources via volatile organic compound observations, Atmospheric Environment, 166, 244-254, 2017.

Li, Z., Walters, W. W., Hastings, M. G., Song, L., Huang, S., Zhu, F., Liu, D., Shi, G., Li, Y., and Fang, Y.: Atmospheric nitrate formation pathways in urban and rural atmosphere of Northeast China: Implications for complicated anthropogenic effects, Environmental Pollution, 296, 118752, https://doi.org/10.1016/j.envpol.2021.118752, 2022.

Lin, Y.-C., Zhang, Y.-L., Yu, M., Fan, M.-Y., Xie, F., Zhang, W.-Q., Wu, G., Cong, Z., and Michalski, G.: Formation mechanisms and source apportionments of airborne nitrate aerosols at a Himalayan-Tibetan Plateau site: Insights from nitrogen and oxygen isotopic compositions, Environmental Science & Technology, 55, 12261-12271, 2021.

Luo, L., Kao, S., Wu, Y., Zhang, X., Lin, H., Zhang, R., and Xiao, H.: Stable oxygen isotope constraints on nitrate formation in Beijing in springtime, Environmental Pollution, 263, 114515, 2020.

Parnell, A. C., Inger, R., Bearhop, S., and Jackson, A. L.: Source partitioning using stable isotopes: coping with too much variation, PloS one, 5, e9672, 2010.

Qiu, X., Ying, Q., Wang, S., Duan, L., Zhao, J., Xing, J., Ding, D., Sun, Y., Liu, B., Shi, A., Yan, X., Xu, Q., and Hao, J.: Modeling the impact of heterogeneous reactions of chlorine on summertime nitrate formation in Beijing, China, Atmos. Chem. Phys., 19, 6737-6747, 10.5194/acp-19-6737-2019, 2019.

Rohrer, F. and Berresheim, H.: Strong correlation between levels of tropospheric hydroxyl radicals and solar ultraviolet radiation, Nature, 442, 184-187, 2006.

Salameh, D., Detournay, A., Pey, J., Pérez, N., Liguori, F., Saraga, D., Bove, M. C., Brotto, P., Cassola, F., and Massabò, D.: $PM_{2.5}$ chemical composition in five European Mediterranean cities: A 1-year study, Atmospheric Research, 155, 102-117, 2015.

Song, W., Wang, Y.-L., Yang, W., Sun, X.-C., Tong, Y.-D., Wang, X.-M., Liu, C.-Q., Bai, Z.-P., and Liu, X.-Y.: Isotopic evaluation on relative contributions of major NO*x* sources to nitrate of $PM_{2.5}$ in Beijing, Environmental Pollution, 248, 183-190, 2019.

Su, X., Tie, X., Li, G., Cao, J., Huang, R., Feng, T., Long, X., and Xu, R.: Effect of hydrolysis of $N_2O_5$ on nitrate and ammonium formation in Beijing China: WRF-Chem model simulation, Science of The Total Environment, 579, 221-229, https://doi.org/10.1016/j.scitotenv.2016.11.125, 2017.

Sun, P., Farley, R. N., Li, L., Srivastava, D., Niedek, C. R., Li, J., Wang, N., Cappa, C. D., Pusede, S. E., and Yu, Z.: $PM_{2.5}$ composition and sources in the San Joaquin Valley of California: A long-term study using ToF-ACSM with the capture vaporizer, Environmental Pollution, 292, 118254, 2022.

https://doi.org/10.5194/egusphere-2025-164
Preprint. Discussion started: 7 March 2025

Tang, G., Yao, D., Kang, Y., Liu, Y., Liu, Y., Wang, Y., Bai, Z., Sun, J., Cong, Z., Xin, J., Liu, Z., Zhu, Z., Geng, Y., Wang, L., Li, T., Li, X., Bian, J., and Wang, Y.: The urgent need to control volatile organic compound pollution over the Qinghai-Tibet Plateau, iScience, 25, 105688, https://doi.org/10.1016/j.isci.2022.105688, 2022.

Vicars, W., Morin, S., Savarino, J., Wagner, N., Erbland, J., Vince, E., Martins, J., Lerner, B., Quinn, P., and Coffman, D.: Spatial and diurnal variability in reactive nitrogen oxide chemistry as reflected in the isotopic composition of atmospheric nitrate: Results from the CalNex 2010 field study, Journal of Geophysical Research: Atmospheres, 118, 10,567-510,588, 2013.

Vicars, W. C. and Savarino, J.: Quantitative constraints on the $^{17}$O-excess ($\Delta^{17}$O) signature of surface ozone: Ambient measurements from 50 N to 50 S using the nitrite-coated filter technique, Geochimica et Cosmochimica Acta, 135, 270-287, 2014.

Walters, W. W., Pye, H. O., Kim, H., and Hastings, M. G.: Modeling the Oxygen Isotope Anomaly ($\Delta^{17}$O) of Reactive Nitrogen in the Community Multiscale Air Quality Model: Insights into Nitrogen Oxide Chemistry in the Northeastern United States, ACS ES&T Air, 2024.

Wang, H., Chen, X., Lu, K., Hu, R., Li, Z., Wang, H., Ma, X., Yang, X., Chen, S., and Dong, H.: $NO_3$ and $N_2O_5$ chemistry at a suburban site during the EXPLORE-YRD campaign in 2018, Atmospheric Environment, 224, 117180, 2020.

Wang, Y., Liu, J., Jiang, F., Chen, Z., Wu, L., Zhou, S., Pei, C., Kuang, Y., Cao, F., and Zhang, Y.: Vertical measurements of stable nitrogen and oxygen isotope composition of fine particulate nitrate aerosol in Guangzhou city: Source apportionment and oxidation pathway, Science of The Total Environment, 865, 161239, 2023.

Wang, Y. L., Song, W., Yang, W., Sun, X. C., Tong, Y. D., Wang, X. M., Liu, C. Q., Bai, Z. P., and Liu, X. Y.: Influences of atmospheric pollution on the contributions of major oxidation pathways to $PM_{2.5}$ nitrate formation in Beijing, Journal of Geophysical Research: Atmospheres, 124, 4174-4185, 2019.

Xia, M., Wang, W., Wang, Z., Gao, J., Li, H., Liang, Y., Yu, C., Zhang, Y., Wang, P., Zhang, Y., Bi, F., Cheng, X., and Wang, T.: Heterogeneous Uptake of $N_2O_5$ in Sand Dust and Urban Aerosols Observed during the Dry Season in Beijing, Atmosphere, 10, 204, 2019.

Xu, Q., Wang, S., Jiang, J., Bhattarai, N., Li, X., Chang, X., Qiu, X., Zheng, M., Hua, Y., and Hao, J.: Nitrate dominates the chemical composition of $PM_{2.5}$ during haze event in Beijing, China, Science of the Total Environment, 689, 1293-1303, 2019.

Yin, M., Guan, H., Luo, L., Xiao, H., and Zhang, Z.: Using nitrogen and oxygen stable isotopes to analyze the major NO*x* sources to nitrate of $PM_{2.5}$ in Lanzhou, northwest China, in winter-spring periods, Atmospheric Environment, 276, 119036, 2022.

Zhang, Q., Zheng, Y., Tong, D., Shao, M., Wang, S., Zhang, Y., Xu, X., Wang, J., He, H., and Liu, W.: Drivers of improved $PM_{2.5}$ air quality in China from 2013 to 2017, Proceedings of the National Academy of Sciences, 116, 24463-24469, 2019.

Zhang, Q., Jiang, X., Tong, D., Davis, S. J., Zhao, H., Geng, G., Feng, T., Zheng, B., Lu, Z., Streets, D. G., Ni, R., Brauer, M., van Donkelaar, A., Martin, R. V., Huo, H., Liu, Z., Pan, D., Kan, H., Yan, Y., Lin, J., He, K., and Guan, D.: Transboundary health impacts of transported global air pollution and international trade, Nature, 543, 705-709, 10.1038/nature21712, 2017.

Zhang, Y.-L., Zhang, W., Fan, M.-Y., Li, J., Fang, H., Cao, F., Lin, Y.-C., Wilkins, B. P., Liu, X., and Bao, M.: A diurnal story of $\Delta^{17}O(NO_3^-)$ in urban Nanjing and its implication for nitrate aerosol formation, npj Climate and Atmospheric Science, 5, 50, 2022.

Zong, Z., Tan, Y., Wang, X., Tian, C., Li, J., Fang, Y., Chen, Y., Cui, S., and Zhang, G.: Dual-modelling-based source apportionment of NO*x* in five Chinese megacities: Providing the isotopic footprint from 2013 to 2014, Environment International, 137, 105592, https://doi.org/10.1016/j.envint.2020.105592, 2020.